# A supercritical $CO_2$ thermal compression cycle enabling power generation from ultra-low waste heat

***Elise Neven[a], Andres Hernandez[b], Gautier Hypolite[c] and Vincent Lemort[d]***

*[a] University of Liège, Liège, Belgium, elise.neven@uliege.be*
*[b] University of Liège, Liège, Belgium, jahernandez@uliege.be*
*[c] Cixten Company, Bischwiller, France, gautier.hypolite@cixten.fr*
*[d] University of Liège, Liège, Belgium, vincent.lemort@uliege.be*

**Abstract:**

Industrial processes generate significant quantities of waste heat that remain unused and represent a major loss of exergy. Studies estimate that between 20% and 50% of the energy input in industrial systems is lost as waste heat, of which a substantial fraction could potentially be recovered. Technologies such as Organic Rankine Cycles and $sCO_2$ Brayton cycles have been developed to convert this waste heat into electricity. However, these conventional systems tend to exhibit reduced thermal efficiency at low-grade temperature levels (<100°C). This paper presents a novel $sCO_2$ power cycle based on a Brayton cycle with thermal compression cycle capable of converting waste heat at temperatures as low as 60°C into electrical power. The proposed system employs a thermal compressor that uses thermal energy rather than mechanical work to compress $CO_2$, enabling improved utilization of low-temperature heat sources. The objective of this study is to evaluate the thermodynamic potential of the proposed cycle in comparison with conventional low-grade heat-to-power technologies and to demonstrate its technical feasibility through first experimental investigations of a prototype. Under identical boundary conditions, the proposed cycle demonstrates higher exergy efficiency than a reference ORC system. In addition, first experimental results obtained from a laboratory-scale prototype confirm the operational feasibility of the concept. Although valve leakage issues limited the full operating range of the prototype, stable operation of the thermal compression principle was successfully demonstrated. These results highlight the potential of the proposed $sCO_2$ cycle for efficient recovery of ultra-low-grade industrial waste heat.

**Keywords:**

Thermal compressor; Supercritical $CO_2$; waste-heat recovery; Experimental prototype.

# 1. Introduction

Waste heat recovery is increasingly recognized as a key lever for industrial decarbonization. A significant fraction of the global energy supply is rejected to the environment as thermal losses, with the industrial sector alone estimated to discharge on the order of 60 EJ per year of waste heat in the world [1]. Low-grade waste heat below 100°C accounts for approximately 40-45% of industrial heat losses [1]. In addition, low-temperature heat sources are also available in renewable systems such as geothermal resources, solar thermal installations, and biomass processes. Despite its abundance, heat below 100°C remains difficult to exploit due to its low exergy content. Converting heat into electricity is an attractive pathway for valorizing these resources, due to the flexibility and transportability of electricity. Several thermodynamic cycles have been proposed for this purpose. For low- and medium- temperature heat sources (below 300°C); Organic Rankine Cycles (ORCs) and their variants are the most widely used technologies. However, their performance deteriorates significantly at heat source temperatures below 100°C, with thermal efficiencies often below 5% [2], which limits their economic viability [3]. Supercritical $CO_2$ Brayton cycles represent another promising technology for waste heat recovery, particularly at higher temperatures (above 400°C [4]). However, their performance is not well suited to low-temperature applications due to the high compression work required relative to expansion work.

As a result, the temperature range of 50-150°C of heat source constitutes a particularly challenging thermodynamic window for heat-to-power conversion. To address these limitations, this work proposes a novel power cycle based on a $CO_2$ Brayton architecture in which mechanical compression is replaced by thermal compression. By using thermal energy to compress the $CO_2$, the proposed configuration aims to:

- Improve net work output at low source temperatures,

- Enhance temperature matching in heat exchangers

The objective of this study is to evaluate the thermodynamic potential of the configuration (section 2), to explain the working principle of the thermal compressor (section 3) and to show the first experimental results of the prototype (section 4).

# 2. Thermodynamical study

## 2.1. $CO_2$ as working fluid: motivation and key properties

Carbon dioxide is an attractive working fluid for thermodynamic cycles due to its low critical temperature (31°C) at a relatively low critical pressure (74 bar). In this regime, $sCO_2$ reaches densities between 200 and 800 kg/m³, which is higher than other gaseous working fluids such as air; thus, for a given mass flow rate, the volumetric flow rate is reduced, enabling more compact turbomachinery and heat exchangers. Despite its high density, $sCO_2$ maintains a relatively low dynamic viscosity, which minimizes frictional pressure losses within components. Furthermore, convective heat transfer is particularly favorable near the critical point, improving heat exchanger performance [5]. From an environmental and safety perspective, $CO_2$ is non-flammable, non-toxic at typical operating concentrations, has a zero ozone depletion potential, and a global warming potential of 1, making it preferable to many synthetic refrigerants. Its abundance, low cost, and wide availability support its practical deployment. Importantly, the low critical temperature enables supercritical operation with relatively low-temperature heat sources, broadening its applicability to wasted heat recovery.

A point of attention when operating with $CO_2$ near its critical point is the strong variation of thermophysical properties along a line often referred to as the pseudo-critical line [6].

## 2.2. Thermal compression interest in $sCO_2$ Brayton cycle

In recent years, increasing research efforts have focused on Brayton cycles operating with $CO_2$ [4]. This growing interest is motivated by the high density of the $CO_2$ near the critical point. As a consequence, the specific volume at the compressor inlet is significantly reduced, which leads to a substantial decrease in compressor work, and, consequently, improves the thermal efficiency [5].

However, a limitation appears when the heat source temperature decreases. Indeed, in this case, the turbine expansion work becomes comparable to the one of the compressor. To illustrate this phenomenon, Figure 1 compares the isentropic compression and expansion processes for two different turbine inlet temperatures ($T_3$=100°C and $T_{3'}$=200°C) in a P-h diagram. For each inlet temperature, the inlet pressure is selected as the highest pressure possible, corresponding to the inflection point of the isotherm ($P_3$= 160 bar and $P_{3'}$= 300 bar). For a turbine inlet temperature of 100°C, the isentropic compression line (red line 1-2) and the isentropic expansion line (red line 3-4) appear nearly parallel in the P-h diagram. As a result, the enthalpy decrease during expansion ($w_{turb,is} = \Delta h_{\mathrm{turb,is}} = h_3 - h_{4,\mathrm{is}}$) is of the same order of magnitude as the enthalpy increase during compression ($w_{comp,is} = \Delta h_{comp,is} = h_{2,\mathrm{is}} - h_1$). Consequently, the net specific work output, defined as $w_{net} = w_{turb,is} - w_{comp,is}$, remains limited. When auxiliary power consumption is additionally considered, the resulting net power output may even become negative. When the turbine inlet temperature increases to 200°C, the slope of the isentropic expansion line is no longer nearly parallel to the isentropic compression line. Under these conditions, the enthalpy drop across the turbine ($\Delta h_{\mathrm{turb,is}} = h_{3'} - h_{4',\mathrm{is}}$) becomes larger than the compressor enthalpy rise ($\Delta h_{comp,is} = h_{2',\mathrm{is}} - h_1$), resulting in a higher net specific work output.

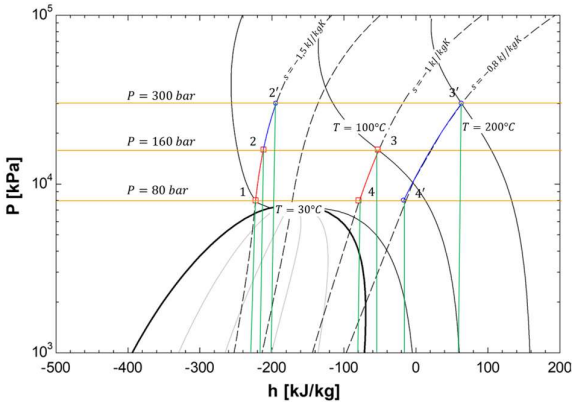


***Figure. 1.*** *Comparison of isentropic compression and expansion specific work at different turbine inlet temperatures and pressures on a $CO_2$ P–h diagram.*

In this context, the use of purely mechanical compression becomes less attractive when the heat source temperature falls below approximately 400°C [4]. To keep the advantages of the Brayton cycle, particularly its favorable temperature matching with secondary heat-transfer fluids, even at lower heat source temperature, another approach consists in replacing the mechanical compression with a thermal one. This is the principle investigated in this work, a Brayton-like cycle in which the conventional mechanical compressor is replaced by a thermal compressor.

## 2.3. Comparison of a Brayton cycle with thermal compression with an ORC

The proposed Brayton cycle with thermal compression is investigated for heat source temperature between 50°C to 150°C. As discussed in the introduction, this temperature range represents a significant and largely untapped source of exergy. For such low heat source temperatures, ORCs currently constitute one of the only technology for power generation [7]. The main exergy losses in ORC systems operating with sensible heat sources occur in the evaporator due to temperature mismatch between the heat source and the working fluid [8]. Pure working fluids evaporate at an almost constant temperature, whereas the heat source (e.g., exhaust gas or geothermal brine) cools continuously as heat is transferred. This mismatch results in large temperature differences during heat exchange, leading to increased entropy generation and exergy destruction. Several approaches have been proposed to mitigate this limitation. These include the use of zeotropic mixtures, transcritical cycles, and trilateral flash cycles. However, these alternative configurations involve system increased complexity and are still largely under development [9].

Therefore, it is relevant to compare the Brayton cycle with thermal compression to the ORC in order to identify the thermodynamic limits of both cycles. The performance of each cycle is evaluated using simplified models developed in Engineering Equation Solver (EES), the main parameters of which are summarized in Table 1. The objective of this analysis is to assess the thermodynamic potential and inherent limitations of both cycles. To this end, only external irreversibilities are considered, while component efficiencies are assumed to be ideal.

Both cycles are analyzed under identical operating conditions, with a heat source temperature $T_{hs}$ of 100°C and a mass flow rate $\dot{m}_{hs}$ of 1,5 kg/s, as well as a heat sink temperature $T_{cs}$ of 20°C. The net electricity production is maximized for each cycle through optimization of the working fluid mass flow rate.

***Table 1.*** *Model parameters for the ORC and Brayton cycle with thermal compression.*

| ORC model | | Brayton cycle with thermal compression model | |
|---|---|---|---|
| Parameter | Value | Parameter | Value |
| Pump efficiency ($\eta_{pp}$) | 100 % | Expander efficiency ($\varepsilon_{is,exp}$) | 100 % |
| Liquid sub-cooling ($\Delta T_{sc}$) | 5 K | Low pressure ($P_{LP}$) | 80 bar |

| | | | |
|---|---|---|---|
| Expander efficiency ($\varepsilon_{is,exp}$) | 100 % | High pressure ($P_{HP}$) | 160 bar |
| Vapour superheating ($\Delta T_{sh}$) | 5 K | Pinch point in exchangers (PP) | 5 K |
| Pinch point in exchangers (PP) | 5 K | | |

For the ORC, the selected working fluid is R1233zd(E), which is widely considered suitable for systems operating within this temperature range [13]. Figure 2 presents both the schematic of the ORC system and its corresponding T-s diagram.

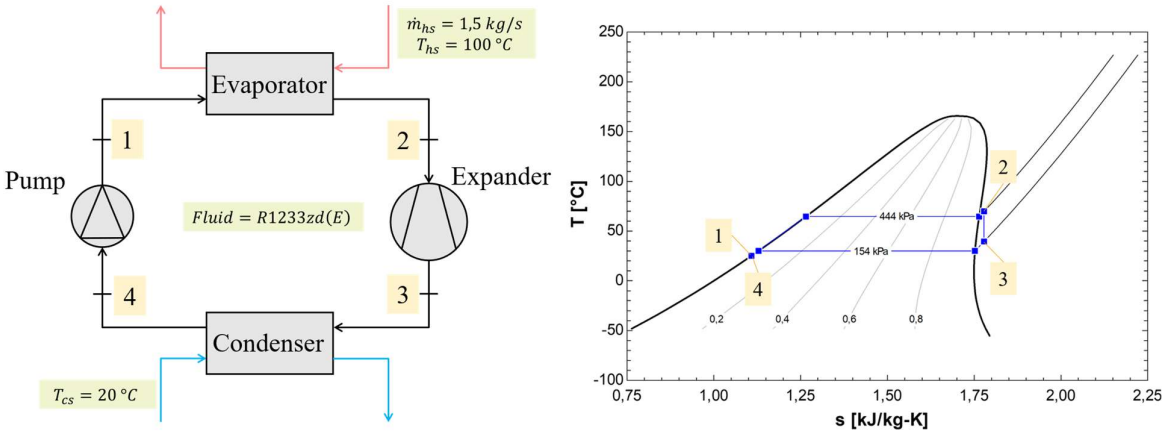


***Figure. 2.*** *Schematic diagram and T-s representation of the ORC.*

For the Brayton cycle, Figure 3 shows both the schematic and the corresponding T-s diagram. The outlet temperature of the thermal compressor ($T_1$) is computed as the average between the minimum and maximum achievable temperature, such that:

$$T_1 = \frac{T_{min} + T_{max}}{2} \tag{1}$$

where $T_{min}$ represents the minimum outlet temperature, determined from the specific volume at the inlet of the thermal compressor, and $T_{max}$ represents the maximum achievable temperature, approximated as $T_2 - 10\ K$. As will be discussed in the following section, the thermal compressor operates cyclically, resulting in a time-dependent variation of its outlet temperature. To avoid dealing with this transient behavior, it is assumed that a large number of thermal compressor modules operate in parallel. This configuration smooths the cyclic fluctuations, allowing the system to be represented by an equivalent steady-state average behavior.

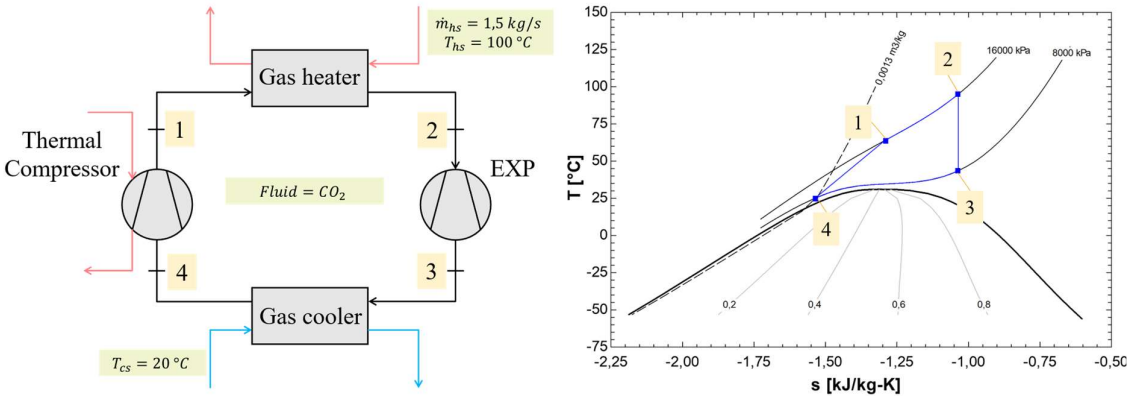


***Figure. 3.*** *Schematic diagram and T-s representation of the Brayton cycle with thermal compression.*

As stated, the selected mass flow rates correspond to those that maximize the net power output. This results in optimal mass flow rates of 1,1 kg/s for the ORC and 2 kg/s for the Brayton cycle. The model results are summarized in Table 2.

***Table 2.*** *Cycles performances.*

| | ORC model | | Brayton cycle with thermal compression model | |
|---|---|---|---|---|
| Net power output | $\dot{W}_{net} = \dot{W}_{exp} - \dot{W}_{pp}$ | 22 kW | $\dot{W}_{net} = \dot{W}_{exp}$ | 50 kW |
| Thermal efficiency | $\eta_{cycle} = \frac{\dot{W}_{net}}{\dot{Q}_{hs}}$ | 9 % | $\eta_{cycle} = \frac{\dot{W}_{net}}{\dot{Q}_{hs}}$ | 14 % |
| Exergy efficiency | $\eta_{ex} = \frac{\dot{W}_{net}}{\dot{X}_{hs}}$ | 5 % | $\eta_{ex} = \frac{\dot{W}_{net}}{\dot{X}_{hs}}$ | 11,5 % |

The exergy rate available at the heat source ($\dot{X}_{hs}$) is computed as follows:

$$\dot{X}_{hs} = \dot{m}_{hs} \cdot ((h_{hs} - h_0) - (T_0 \cdot (s_{hs} - s_0)) \quad (2)$$

where the reference temperature $T_0$ is set to 25°C and the reference pressure $P_0$ corresponds to atmospheric conditions.

The results indicate a clear advantage for the Brayton cycle with thermal compression. This can be attributed to its ability to extract a larger amount of heat from the source and the reduction of the exergy destruction in the high-temperature heat exchanger. Figure 4 shows the temperature profile evolution in the evaporator for the ORC and in the thermal compressor and the gas heater for the Brayton cycle.

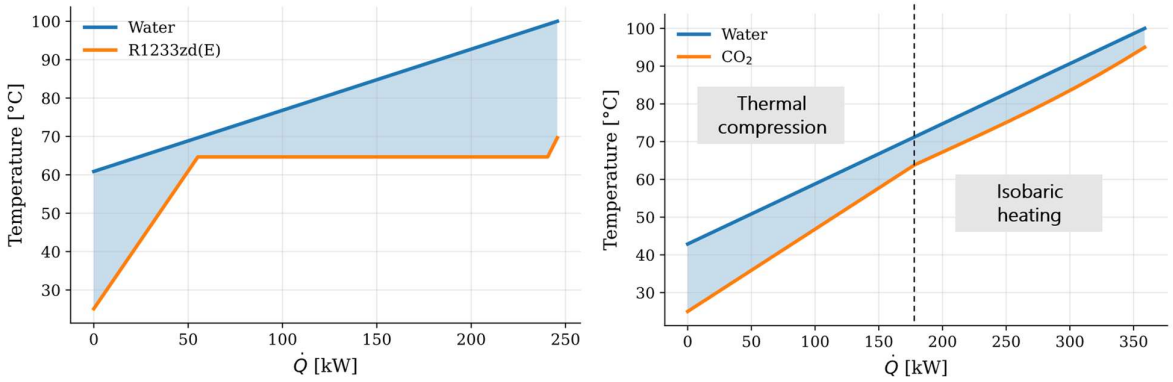


***Figure. 4.*** *Temperature-heat transfer diagram of the evaporator in the ORC (left) and of the thermal compressor and gas heater in the Brayton cycle (right) where the dotted line represents the separation between the thermal compressor and the gas heater.*

# 3. System working principle

## 3.1. Thermal compression cycle

A thermal compressor (also called a thermocompressor) is a device that uses thermal energy to increase the pressure of a working fluid. The most widely used thermocompressors are ejectors and percolator pumps [10].

The thermal compressor investigated in this study is based on a Stirling-type compression cycle. In contrast to a conventional Stirling engine, the Stirling thermal compressor operates as an open system in which the power piston is replaced by two valves: an inlet valve allowing fluid admission and an outlet valve allowing discharge at high pressure. The earliest mention of a Stirling-based thermal compressor was proposed by

Bush [11]. More recently, related concepts have been explored in practical applications such as those developed in [12].

Figure 5 illustrates the main components of a module of the studied thermal compressor. The system consists of an internal cavity filled with $CO_2$, referred to as the working chamber, two heat exchangers, a displacer and two valves. The working chamber is thermally coupled to both a hot and a cold heat exchanger, where cold and hot water circulate around the cavity. The system also includes a displacer, which transfers the $CO_2$ between the hot and cold regions of the working chamber, enabling cyclic heating and cooling. A supply check valve allows fluid to enter the system, while an exhaust valve controls the discharge of the compressed fluid.

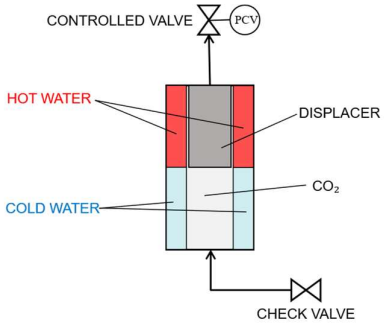


***Figure. 5.*** *Thermal compressor's schematic representation.*

Figure 7 illustrates the evolution of the thermal compression cycle, which consists of four evolutions corresponding to different positions of the valves and the displacer.

- **A: Initial state:** At the initial state of the cycle (state A), the chamber contains the maximum mass of $CO_2$ ($M_{max} = M_0 + \Delta M$) at low pressure and low temperature.
- **A-B: Isochoric compression:** The displacer moves the $CO_2$ from the cold region towards the hot region of the chamber. During this step, both valves remain closed, so the process occurs at constant volume. Heat is transferred from the hot water surrounding the cavity to the $CO_2$, increasing its temperature (from 20°C to 35°C) and rising the pressure from the minimal pressure (80 bar) to the maximum one (160 bar). During this phase, the mass remains constant ($M_{max}$).
- **B-C: Isobaric discharge:** Once the targeted high pressure is reached (160 bar), the discharge valve PCV (which stands for pressure control valve) opens and high-pressure $CO_2$ is discharged from the chamber. During this process, the mass of $CO_2$ decreases from its maximum value to its minimum value, corresponding to the discharge amount $\Delta M$. The temperature continues to increase due to the ongoing heat transfer from the hot source.
- **C-D: Isochoric cooling:** When the minimum mass of $CO_2$ is reached, PCV closes. The displacer then transfers the remaining $CO_2$ from the hot to the cold region of the cavity. Heat is removed by the cold water circulating around the cylinder, leading to a decrease in temperature and pressure, bringing the high-pressure back to the low-pressure level of the cycle.
- **D-A: Isobaric intake:** When the pressure inside the chamber reaches the low-pressure, the check valve opens. Fresh $CO_2$ enters the chamber at constant pressure. The cavity is refilled with the mass $\Delta M$ until the maximum mass is restored.

The temperature and pressure values used are to illustrate the order of magnitudes. Both the high pressure and the pressure ratio are parameters that should be optimized according to the external operating conditions. The P-v diagram of the cycle is shown in Figure 6.

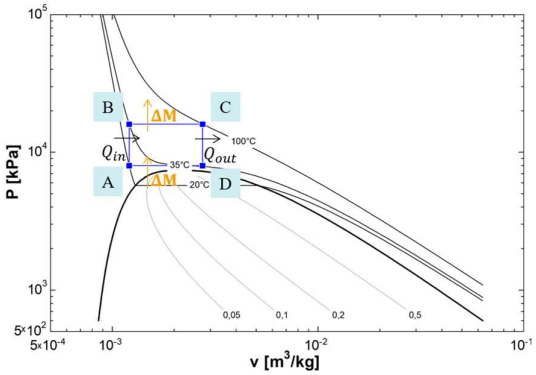


***Figure. 6.*** *P-v diagram of thermal compression cycle.*

| State A | State A->B | State B->C | State C->D | State D->A |
|---|---|---|---|---|
| Position 0 | Position 1 | Position 2 | Position 3 | Position 4 |
| 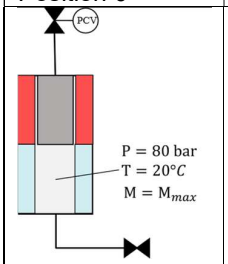 | 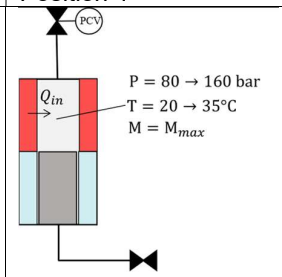 | 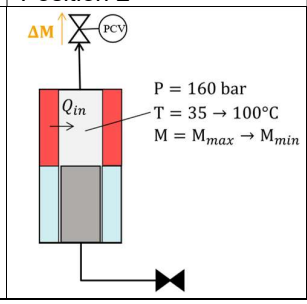 | 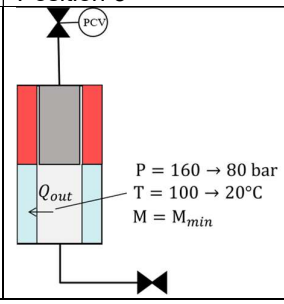 | 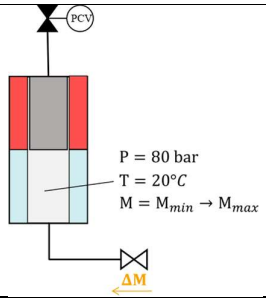 |



***Figure. 7.*** *Evolutions of the thermal compression cycle.*

The displacer may also act as a regenerator, temporarily storing and releasing thermal energy and thereby improving the efficiency of the thermal compression process. During the A-B isochoric compression phase, the $CO_2$ can be preheated when passing around the displacer. In this paper configuration, heat transfer occurs only through the external metallic surface of the displacer. In future work, the displacer could be made of porous material to increase its thermal capacity and enhance the regenerative effect.

For further technical details about this thermal compressor, refer to the patent of the Cixten company [14].

## 3.2. Thermal compressor sequence

To ensure a relatively smooth mass flow rate at the thermal compressor outlet, two modules operating according to the cycle described in the previous section are employed and run in opposite phase; together, they constitute the thermal compressor. While the previous section presented an idealized thermodynamic cycle, in practise, the isochoric cooling process (C-D) and the isobaric intake process (D-A) occur simultaneously (at valve and displacer positions corresponding to the position 4 of Figure 7). The operating sequence of the two modules is illustrated in Figure 8. This sequence is made to have a mass flow rate as smooth as possible at the thermal compressor outlet. Increasing the number of modules further reduces fluctuations in both mass flow rate and outlet temperature.

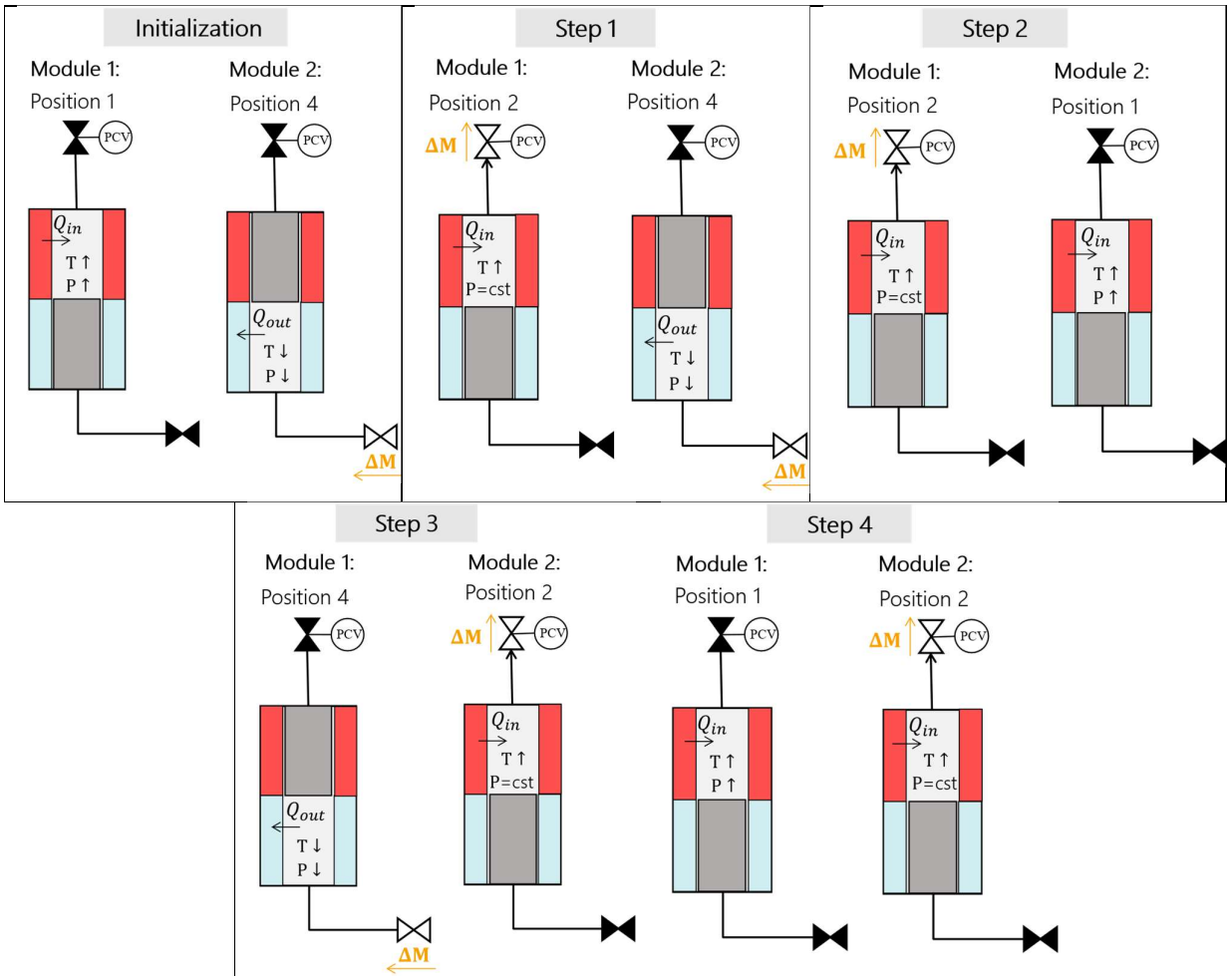


***Figure. 8.*** *Representation of the sequence of the thermal compressor using two modules.*

## 3.3. Integration of the thermal compressor in the Brayton cycle

The complete system consists of four main components: a thermal compressor, a gas heater, an expander, and a gas cooler (see Figure 3). One of the key advantages of this concept lies in its modularity, as the system power output can be adjusted by adding or removing thermal compressor modules.

A major challenge associated with this cycle is the difference in operating regimes between components. While the gas heater, expander, and gas cooler operate under quasi-steady-state conditions, each thermal compressor module undergoes a cyclic sequence of filling, heating, and discharge. As a result, the thermodynamic state at the outlet of the compressor varies over time during the discharge phase (B->C).

This behavior is illustrated in Figure 9, which presents the T-s diagram of the cycle at two distinct moments of the discharge process: (i) the beginning of the isobaric discharge (corresponding to state B in the thermal compression cycle), and (ii) at the end of the isobaric discharge (corresponding to state C).

During the discharge of one of the thermal compressor module, state 1 is the only state that varies dynamically, while the remainder of the cycle can be approximated as operating under steady-state conditions. This is due to the gas heater that brings the $CO_2$ to a temperature $T_2$. The temperature $T_1$ increases during the isobaric discharge as the working fluid is still heated in the module while being expelled. Once the discharge is complete, the pressure control valve (PCV) of the active module closes, while that of the second module opens. This transition causes the system to return to the minimum inlet temperature $T_1$, as illustrated in Figure 9 (left).

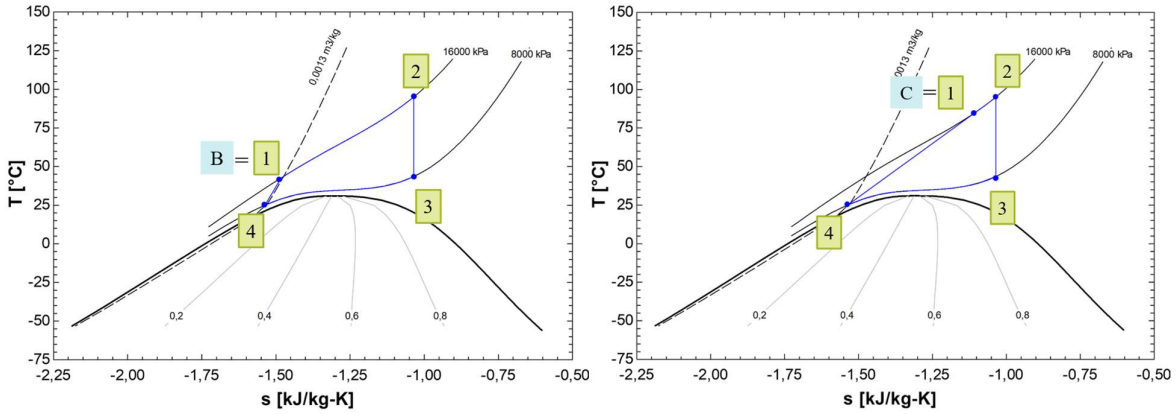


***Figure. 9.*** *Ts diagram of the Brayton cycle at the beginning of the discharge of one module (left) and at the end of the discharge of the same module (right).*

# 4. Experimental validation

To demonstrate the concept of the Brayton cycle using a thermal compression cycle, a prototype was developed by Cixten and subsequently completed and tested at the University of Liège.

## 4.1. Test bench description

The experimental test bench is designed to investigate the performances and feasibility of the proposed cycle. The P&ID is represented in Figure 10.

**CO2 Loop**

The $CO_2$ loop includes the following main components: a thermal compressor, a gas heater (EX01), an expansion device, a gas cooler (EX02). The $CO_2$ follows the same thermodynamic evolutions as in Figure 3.

After the gas heater, the loop splits into three alternative expansion branches:

1. Manual expansion valve branch (VLV01) – used during the initial commissioning and primary tests.
2. Scroll expander branch (EXP) – intended for future power production experiments
3. Expansion valve (VLV02) in series with a heat exchanger (EX03) branch – used to reproduce the behavior of the scroll expander.

In the present study, only the third branch (expansion valve combined with EX03) is used. This configuration allows to test the thermal compressor while maintaining stable and controllable conditions before conducting experiments with the scroll expander.

A liquid receiver (LR) is installed upstream of the thermal compressor to stabilize the mass flow rate and dampen flow fluctuations caused by the batch operation of the compressor modules. The gas heater (EX01) and the gas cooler (EX02) are double-pipe counter-current heat exchangers while the third heat exchanger (EX03) is a brazed plate heat exchanger. The expansion valve VLV02 is a pneumatic valve.

**Heat source circuit**

The heat source is provided by a hot water loop supplied by an oil-boiler. To achieve precise control of the experimental conditions, recirculation loops are implemented. These allow the mass flow rate and inlet temperature of the water entering both the thermal compressor and the gas heater to be adjusted independently.

**Heat sink circuit**

The heat sink is provided by tap water. Similar to the hot water loop, recirculation loops are used to independently regulate the temperature and mass flow rate of the cooling water entering the heat exchangers EX02, EX03 and the thermal compressor.

**Instrumentation and data acquisition**

The system is instrumented with temperature (TT), pressure (PT) and mass flow (FT) sensors installed at key locations in the cycle. All measurements and control functions are managed using LABVIEW and a compact-RIO acquisition system.

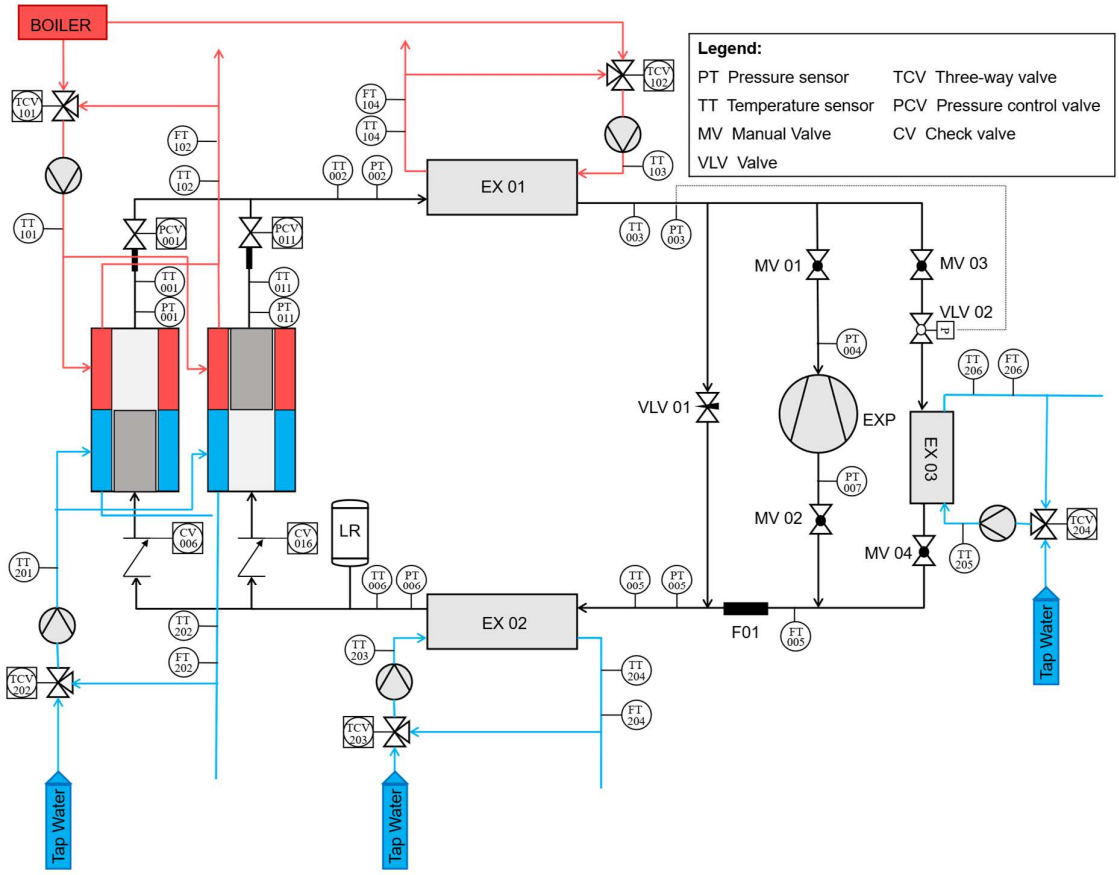


***Figure. 10.*** *P&ID of the prototype of the Brayton-like cycle with thermal compression.*

## 4.2. Experimental tests

Initial experimental tests were conducted to validate the operation of the prototype thermal compressor and the overall test bench. During the first experimental campaigns, several technical issues were identified. In particular, the pressure control valves (PCV001 and PCV011) installed on the thermal compressor modules were not perfectly leak-tight, allowing a portion of the CO2 mass flow to circulate between the two compressor modules instead of flowing through the expansion branch. Indeed, the Coriolis flow meter (FT005) indicated an almost zero mass flow rate, suggesting that an important part of the CO2 flow was bypassing the measurement section. Despite these issues, the experiments provided valuable insight into the dynamic pressure behaviour of the system, which is a key aspect of the system operation.

**Pressure dynamics during a thermal compression cycle**

The evolution of the pressures during a complete operating sequence of the thermal compressor is shown in Figure 11. For these tests, the pressure setpoint was fixed at 130 bar. The PCV were therefore configured to open when the pressure inside a module reached this value. A first observation is that the pressure inside the modules (PT001 and PT011) slightly exceeds the setpoint pressure before the valve opens. This behavior is due to the response time of the control valve, which causes a small pressure overshoot before the discharge process begins.

From a system perspective, an important observation is that the pressure at the outlet of the thermal compressor (PT003), which corresponds to the inlet pressure of the expansion branch, remains relatively stable throughout the sequence. Achieving a quasi-steady pressure at this location is one of the objectives, as it allows the downstream components to operate under nearly steady conditions despite the batch operation of the compressor modules. However, the measured pressure level at PT003 is lower than expected. Ideally, this pressure should stabilize at a value close to the peak pressure reached inside the compressor modules. This phenomenon observed in the experiments is mainly attributed to the mass transfer occurring between the two modules, which reduced the pressure levels in the rest of the cycle.

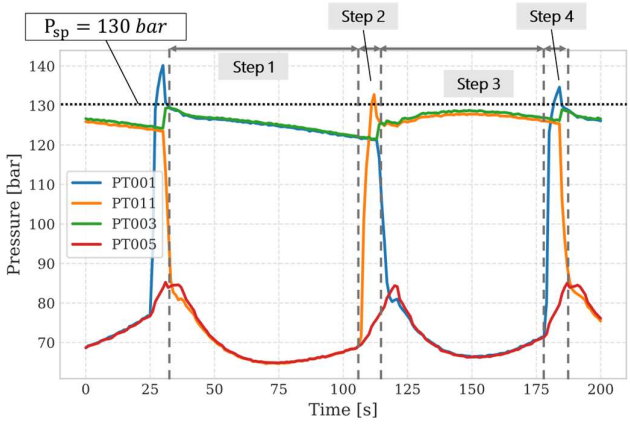


***Figure. 11.*** *Evolution of the pressures in the cycle. PT001 : pressure inside the first module; PT011 : pressure inside the second module; PT003 : pressure after the gas heater; PT005 : pressure after the expander.*

**Influence of the expansion valve opening**

Figure 12 presents the evolution of the CO2 temperatures and pressures during a complete experimental campaign. The results highlight the impact of the opening of the expansion valve (VLV02 on the P&ID and EV in Figure 12) on the pressure distribution in the system. When the expansion valve opening is set to 20%, the pressure ratio between the inlet and outlet of the expansion branch (PT003/PT005) is relatively low. As the valve opening increases (e.g., to 25%), the corresponding pressure ratio increases. This behavior indicates that flow restriction induced by the expansion device influences the operating pressure of the entire cycle. In future experiments, when the scroll expander replaces the expansion valve, the rotational speed of the expander will play a similar role, determining the pressure ratio.

**Operational optimization**

The performance of the system will ultimately depend on the optimal combination of the pressure setpoint of the thermal compressor and the operating speed of the expander. These parameters must be adjusted according to the external boundary conditions.

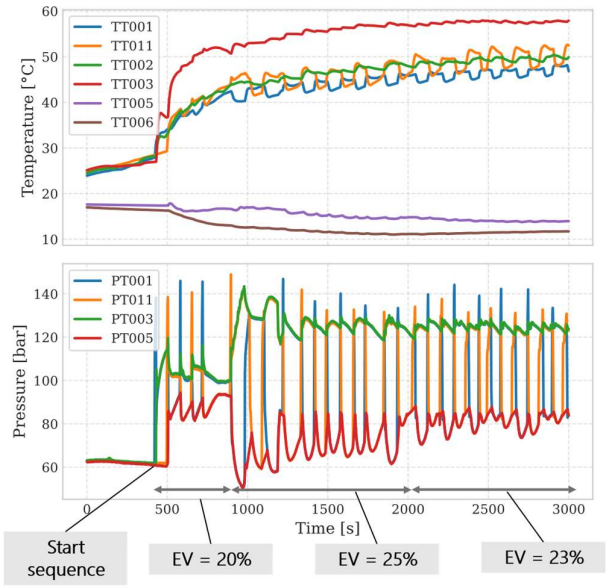


***Figure. 12.*** *Evolution of the temperatures and pressures in the cycle over an entire experimental campaign. EV represents the expansion valve opening.*

# 5. Conclusions

This paper presents a novel thermal compressor prototype designed to operate in a Brayton-like power cycle for electricity generation from low-temperature heat source (below 150°C). The proposed cycle is first analyzed from a thermodynamic perspective and compared with conventional power cycles commonly used for low-temperature heat recovery, namely the conventional Brayton cycle and the ORC. In a conventional $sCO_2$ Brayton cycle operating with heat source below approximately 400°C, mechanical compression becomes unfavorable, as the compression work approaches the magnitude of the expansion work, resulting in a very limited net power output. In contrast, the proposed cycle replaces mechanical compression with thermal compression. Compared with the ORC, the proposed cycle shows a better utilization of the heat source, leading to better exergy efficiencies (11,5 % instead of 5%).
The operating principle of the thermal compressor is then described, together with its impact on the overall cycle operation. Due to the batch operation of the compressor modules, the outlet state of the thermal compressor exhibits dynamic behavior, while the rest of the cycle can be approximated as quasi-steady.

Finally, first experimental results obtained from a prototype test bench are presented. These results demonstrate the feasibility of the proposed concept, although several technical issues were identified during the experiments. In particular, leakage issues in the pressure control valves affected the system operation and let to internal mass transfer between the compressor modules.

Future work will focus on a more detailed characterization of the prototype, with the objective of identifying the optimal operating conditions of the cycle under varying boundary conditions.

# Nomenclature

$h$ specific enthalpy, kJ/kg
$\dot{m}$ mass flow rate, kg/s
$T$ temperature, °C
w specific work, kJ/kg
$\dot{W}$ work power, kW
$\dot{X}$ exergy transfer, kW

$\eta$ efficiency [%]
$\varepsilon$ effectiveness [%]
$hs$ heat source
$exp$ expander
$pp$ pump

# References

[1] C. Forman, I. K. Muritala, R. Pardemann, and B. Meyer, 'Estimating the global waste heat potential', *Renewable and Sustainable Energy Reviews*, vol. 57, pp. 1568–1579, May 2016, doi: 10.1016/j.rser.2015.12.192.

[2] F. D. Sánchez, J. Barba Salvador, and C. Mata Montes, 'Organic Rankine Cycle System Review: Thermodynamic Configurations, Working Fluids, and Future Challenges in Low-Temperature Power Generation', *Energies*, vol. 18, no. 24, p. 6561, Dec. 2025, doi: 10.3390/en18246561.

[3] D. Walraven, B. Laenen, and W. D'haeseleer, 'Minimizing the levelized cost of electricity production from low-temperature geothermal heat sources with ORCs: Water or air cooled? , *Applied Energy*, vol. 142, pp. 144–153, Mar. 2015, doi: 10.1016/j.apenergy.2014.12.078.

[4] Y. Liu, Y. Wang, and D. Huang, 'Supercritical CO2 Brayton cycle: A state-of-the-art review', *Energy*, vol. 189, p. 115900, Dec. 2019, doi: 10.1016/j.energy.2019.115900.

[5] Y. Ahn *et al.*, 'Review of supercritical CO2 power cycle technology and current status of research and development', *Nuclear Engineering and Technology*, vol. 47, no. 6, pp. 647–661, Oct. 2015, doi: 10.1016/j.net.2015.06.009.

[6] Martin T. White, Giuseppe Bianchi, Lei Chai, Savvas A. Tassou, and Abdulnaser I. Sayma. "Review of Supercritical CO2 Technologies and Systems for Power Generation". In: Applied Thermal Engineering (Feb. 25, 2021). doi: 10.1016/j.applthermaleng.2020.116447.

[7] L. Liu, Q. Yang, and G. Cui, 'Supercritical Carbon Dioxide(s-CO2) Power Cycle for Waste Heat Recovery: A Review from Thermodynamic Perspective', *Processes*, vol. 8, no. 11, p. 1461, Nov. 2020, doi: 10.3390/pr8111461.

[8] T. Klamrassamee, T. Kittijungjit, Y. Sukjai, and Y. Laoonual, 'Thermodynamic, economic, and carbon emission evaluation of various Organic Rankine cycle configurations for maximizing waste heat recovery potential', *Energy Conversion and Management: X*, vol. 26, p. 100943, Apr. 2025, doi: 10.1016/j.ecmx.2025.100943.

[9] S. Quoilin, M. V. D. Broek, S. Declaye, P. Dewallef, and V. Lemort, 'Techno-economic survey of Organic Rankine Cycle (ORC) systems', *Renewable and Sustainable Energy Reviews*, vol. 22, pp. 168–186, Jun. 2013, doi: 10.1016/j.rser.2013.01.028.

[10] A. A. Kornhauser, 'Analysis of an idealized Stirling thermocompressor', in *IECEC 96. Proceedings of the 31st Intersociety Energy Conversion Engineering Conference*, Washington, DC, USA: IEEE, 1996, pp. 1331–1336. doi: 10.1109/IECEC.1996.553909.

[11] Walker, G., 1980, Stirling Engines, Clarendon Press, oxford, pp121-123.

[12] Ibsaine, R. (2015). Étude d'un système tritherme intégrant une compression thermique originale, destiné au marché du chauffage résidentiel. PhD thesis. Thèse de doctorat dirigée par Stouffs, Pascal Energétique Pau 2015.

[13] S. Eyerer, C. Wieland, A. Vandersickel, and H. Spliethoff, 'Experimental study of an ORC (Organic Rankine Cycle) and analysis of R1233zd-E as a drop-in replacement for R245fa for low temperature heat utilization', *Energy*, vol. 103, pp. 660–671, May 2016, doi: 10.1016/j.energy.2016.03.034.

[14] Pierre-Yves Berthélémy. "Cartridge for a Heat Engine Having a Thermodynamic Cycle and Associated Heat Engine". U.S. pat. 2025/0116212A1. Apr. 10, 2025. url: https://worldwide. espacenet . com / publicationDetails / biblio ? DB = EPODOC & II = 0 & ND = 3 & adjacent = true & locale = fr _ EP & FT = D & date = 20250410 & CC = US & NR = 2025116212A1 & KC = A1 (visited on 12/03/2025).